DOI: 10.1002/cssc.201402474

Monitoring Solid Oxide CO_2 Capture Sorbents in Action

Christopher J. Keturakis,[a] Fan Ni,[b] Michelle Spicer,[b] Michael G. Beaver,[b] Hugo S. Caram,[b] and Israel E. Wachs*[a]

The separation, capture, and storage of CO_2, the major greenhouse gas, from industrial gas streams has received considerable attention in recent years because of concerns about environmental effects of increasing CO_2 concentration in the atmosphere. An emerging area of research utilizes reversible CO_2 sorbents to increase conversion and rate of forward reactions for equilibrium-controlled reactions (sorption-enhanced reactions). Little fundamental information, however, is known about the nature of the sorbent surface sites, sorbent surface–CO_2 complexes, and the CO_2 adsorption/desorption mechanisms. The present study directly spectroscopically monitors Na_2O/Al_2O_3 sorbent–CO_2 surface complexes during adsorption/desorption with simultaneous analysis of desorbed CO_2 gas, allowing establishment of molecular level structure–sorption relationships between individual surface carbonate complexes and the CO_2 working capacity of sorbents at different temperatures.

Introduction

The separation, capture, and storage of CO_2, the major greenhouse gas, from industrial gas streams has received considerable attention in recent years due to concerns about the environmental effect of increasing CO_2 concentration in the atmosphere. The characteristics of different sorbents (zeolites, silica gels, aluminas, and activated carbons with promoters ranging from alkali and alkaline earth metals to amines) and their potential applications have recently been reviewed.[1,2] An emerging area of research utilizing reversible CO_2 sorbents is the novel sorption enhanced reaction (SER) that circumvents the thermodynamic limitations (purity and conversion) of equilibrium-controlled reactions by selectively removing a reaction product from the gas phase and increasing the conversion and rate of the forward reaction.[3] For example, during the manufacture of H_2 from natural gas, the major industrial process for H_2 production, CO_2 sorbents are able to shift the reaction equilibrium to the right, thus,

$$CH_4 + 2\,H_2O \leftrightarrow 4\,H_2 + CO_2 \qquad (1)$$

allowing for increased production of hydrogen in the process.[1]

Lee et al. has recently studied two promising high temperature chemisorbents for the water–gas-shift-SER (WGS-SER), a K_2CO_3-promoted hydrotalcite and a Na_2O-promoted alumina.[1,4–7] The chemisorbents were originally developed by Air Products and Chemicals, Inc. to produce fuel-cell-grade hydrogen by steam methane reforming.[8–11] These chemisorbents offer (i) reversible sorption of CO_2 in the presence of steam, H_2, and CO, (ii) relatively fast CO_2 sorption and desorption kinetics, (iii) moderate heats of sorption (~20–65 kJ mol^{-1}), (iv) acceptable cyclic working capacity, (v) nearly infinite selectivity of CO_2 chemisorption over gases like CO, steam, N_2, and CH_4 at 200–500 °C, and (vi) thermal stability under WGS reaction conditions.

$$H_2O + CO \leftrightarrow H_2 + CO_2 \qquad (2)$$

A comparison between the two sorbents indicated that Na_2O-promoted alumina requires about 50% less steam for regeneration. A new analytical model for these sorbents was derived by Lee et al. to describe the deviation from conventional Langmuirian equilibrium chemisorption isotherms.[4] This model, though it described the data well, assumed, without experimental proof, that there is one single type of adsorption site and that deviations from the Langmuir model are due to complexing between the gas and already chemisorbed CO_2 molecules. These sorbents have been donated by Air Products and Chemicals, Inc. to Lehigh University for further development.

Similar chemisorbents based on CaO (Periodic group II) and CaO-promoted alumina have also been explored by other authors.[1,12–18] These CaO-based chemisorbents appear to have similar working capacities, tolerance to steam, and cyclic working capacities, but poorer regeneration capabilities compared to their Na_2O (periodic group I)-based counterparts. At the time of writing, only one study by Duyar et al. has demonstrated that support CaO sorbents can be regenerated at temperatures as low as 350 °C.[18]

[a] C. J. Keturakis, Prof. I. E. Wachs
Operando Molecular Spectroscopy and Catalysis Laboratory
Department of Chemical Engineering
Lehigh University
Bethlehem, PA 18015 (USA)
E-mail: iew0@lehigh.edu

[b] F. Ni, M. Spicer, Dr. M. G. Beaver, Prof. H. S. Caram
Department of Chemical Engineering
Lehigh University
Bethlehem, PA 18015 (USA)

Supporting Information for this article is available on the WWW under http://dx.doi.org/10.1002/cssc.201402474.

Promoted aluminas for catalysis have been extensively studied in the literature, though most studies focus on promotion with transition-metal oxides rather than alkali-metal oxides.[19–27] It is now well established that transition-metal oxides are highly dispersed at low loadings on alumina and form 2D monolayers consisting of isolated sites, dimers, or polymers by titrating the surface alumina hydroxyls. Increasing the dopant loading above monolayer coverage (titration of all hydroxyls) ushers the formation of 3D metal-oxide nanoparticles. The formation of active sites for alkali and alkaline earth metal-oxide dopants, which tend to display ionic character, is still not well understood.

Gruene et al. characterized a CaO/Al_2O_3 sorbent by in situ IR spectroscopy, thermogravimetric analysis (TGA), and XRD.[15] Neither XRD nor IR spectroscopy detected any crystalline phases, such as CaO, $CaCO_3$, or mixed CaAl oxides, at loadings as high as 20.3 wt% CaO/Al_2O_3, indicating that the calcium phase is highly dispersed with a small domain size. The TGA results suggested that multiple adsorbed carbonate species exist on the sorbent surface, but IR spectroscopy could not distinguish them and only one chemisorbed carbonate species could be detected. Previous studies on CaO/Al_2O_3 also reached the same conclusion from Raman and IR spectroscopy, XRD, and X-ray photoelectron spectroscopy (XPS); the calcium phase is highly dispersed and not detectable as CaO, though minor amounts of $CaCO_3$ are sometimes detected.[28,29] A recent $CaO–Al_2O_3$ mixed oxide study corroborated the same results.[30]

Potassium, a group I alkali metal, is expected to exhibit similar surface molecular structures as sodium when impregnated on alumina. The K_2O/Al_2O_3 system has recently garnered renewed attention as a NO_x storage material utilized at high temperatures and it has been shown that the potassium surface phases present depend on the precursor used.[31–34] A nitrate precursor forms rhombohedral KNO_3 and orthorhombic KNO_3 below 300 °C. Above 300 °C, the KNO_3 phase decomposes to an amorphous phase and sometimes minor K_2O is detected.[33,34] Non-nitrate precursors form K_2CO_3 at high calcination temperatures and sometimes a minor amount of K_2O.[32] For samples calcined above 300 °C, XPS of the K 2p region revealed that approximately 60% of potassium is in the K^+ ionic form and approximately 40% is in the form of a K–O bond. The molecular structure of K_2O/Al_2O_3 calcined above 300 °C has still not been determined.

Early sodium-promoted alumina studies concluded that sodium addition consumes the alumina hydroxyls, alumina hydroxyls become more basic in character with increasing sodium loading, and Lewis acid centers are eliminated.[35–38] Very little fundamental information is known about the Na_2O/Al_2O_3 system such as the nature of the sorbent surface sites, sorbent surface–CO_2 complexes and the CO_2 adsorption/desorption characteristics.

In the present study we characterize Na_2O/Al_2O_3 solid sorbents using in situ Raman and IR molecular vibrational spectroscopy, and TGA for determining adsorption/desorption characteristics and sorbent–CO_2 working capacity at different temperatures. Specific temperatures of interest are 200 and 400 °C, which correspond to the reaction conditions of the low and high temperature WGS. At these temperatures physisorbed CO_2 cannot exist and, thus, it is chemisorbed CO_2 that is responsible for the working capacity of the sorbents. The sorbent–CO_2 surface complexes in action were monitored with operando temperature programmed-IR (TP-IR) spectroscopy, IR spectroscopy of the sorbent–CO_2 surface complexes with simultaneous analysis of desorbed CO_2 gas with online mass spectrometry (MS), allowing establishment of structure–sorption relationships between individual surface carbonates and the CO_2 working capacity of the sorbents at high temperatures.

Results and Discussion

The 1–9 wt% Na_2O/Al_2O_3 sorbents were synthesized by incipient wetness impregnation of aqueous solutions of sodium hydroxide (NaOH) onto γ-Al_2O_3. Results from Brunauer–Emmett–Teller (BET) surface area analysis, given in Table 1, indicate a systematic decrease in surface area, within error, with increasing Na_2O loading. The anchoring sites of Na_2O on the surface hydroxyls of the alumina were monitored with in situ IR spectroscopy and the resulting spectra of the surface hydroxyl region are shown in Figure 1 as a function of Na_2O loading. The surface hydroxyls on pure γ-alumina have been extensively studied and reviewed using modern density functional theory (DFT) calculations.[39,40] The γ-alumina employed in the present study contains five distinct surface hydroxyls and their assignments are given in Table S1 of the Supporting Information. Upon addition of 1% Na_2O, the complete consumption of the HO-μ_1-Al_{VI} surface hydroxyls (vibration at 3760 cm^{-1}) takes place (Note: Al_V/Al_{VI} indicates a 5/6-coordinated Al atom and μ_2/μ_3 indicates that the OH is bonded to two/three Al_{xx} atoms). The IR intensity of the HO-μ_2-Al_{VI} and HO-μ_3-Al_{VI} surface hydroxyls vibrating at 3675 and 3566 cm^{-1}, respectively, also decrease with Na_2O addition (see Figure 1 inset). The intensity of the IR bands vibrating at 3734 and 3720 cm^{-1} remain nearly unchanged up to 3% Na_2O, indicating a preferential consumption of the other surface hydroxyls. On increasing loading to 5% Na_2O/Al_2O_3, the HO-μ_1-Al_V and H_2O-μ_1-Al_V, the surface hydroxyls that exhibit IR bands at 3734 and 3720 cm^{-1}, respectively, are consumed. For the 7% and 9% Na_2O/Al_2O_3 sorbents, the surface hydroxyls no longer change with increasing

Table 1. Sorbent calculated surface density and measured BET surface area.

Sample	Surface density [Na atoms nm^{-2}]	BET surface area [$m^2 g^{-1}$]
γ-Al_2O_3	–	200
1% Na_2O/Al_2O_3	0.98	186
2% Na_2O/Al_2O_3	1.98	163
3% Na_2O/Al_2O_3	3.00	166
5% Na_2O/Al_2O_3	5.11	175
7% Na_2O/Al_2O_3	7.31	161
9% Na_2O/Al_2O_3	9.61	148

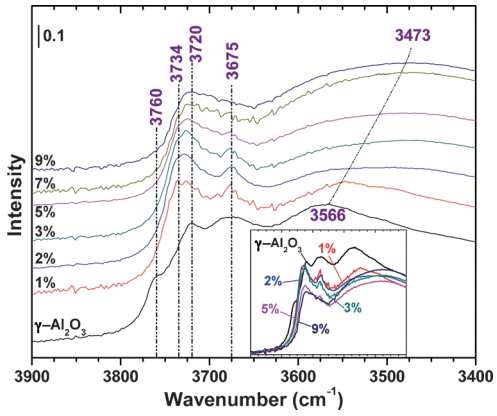

Figure 1. In situ DRIFTS of the hydroxyl region for dehydrated *x*% Na_2O/Al_2O_3 sorbents at 200 °C. Spectra are vertically offset to aide in distinguishing surface hydroxyls. Inset: Selected spectra stacked on top of each other to demonstrate the consumption of surface hydroxyls with increasing Na_2O loading.

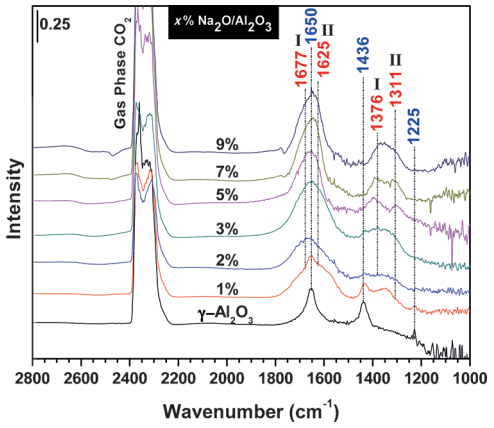

Figure 2. In Situ DRIFTS of CO_2 adsorption at 200 °C on *x*% Na_2O/Al_2O_3 sorbents. The corresponding IR spectrum of each dehydrated sample was subtracted from all spectra during CO_2 adsorption.

sodium oxide loading and crystalline Na_2CO_3 nanoparticles (NPs) appear in the corresponding in situ Raman and IR spectra (see Supporting Information, Figures S3 and S4). The experimental observation of Na_2CO_3 3D NPs above monolayer coverage of surface carbonate species indicates saturation of the surface Na_2O monolayer. The remaining, broad surface hydroxyl IR band at 3720 cm^{-1} corresponds to a thermally stable water group that does not dissociate into a hydroxyl, H_2O-μ_1-Al_V, which is likely the reason it is not fully consumed.[40]

The vibration of the bridging Na–O–support bond is not observed in the Raman spectra of the Na_2O/Al_2O_3 sorbents (see Supporting Information, Figure S3), suggesting that the bond is ionic in character as ionic bonds are not Raman active. Given sodium's penchant for forming ionic bonds, it seems likely that sodium anchors by titrating the alumina surface hydroxyls by displacing the hydrogen and forming a Na^+ ion and a counter $Al–O^-$ ion. This imparts a greater nucleophilic/basic character to the oxygen atom. Crystalline sodium aluminate phases (main Raman bands at 440 and 490–500 cm^{-1}) or NaO_x phases (200–600 cm^{-1}) were also not detected in the Raman spectra indicating its absence in these Na_2O/Al_2O_3 sorbents.[41,42]

The basic Na_2O/Al_2O_3 sorbent was surprisingly found to already contain strongly bound acidic CO_2, which was captured from ambient air and could not even be liberated by air calcination at 400 °C for 2 h. In situ Raman and IR spectroscopic analyses show that the strongly bound surface CO_2 and CO_3^{2-} consist of linear CO_2 on all samples and two polydentate carbonates (CO_3-μ_3-Al), labeled polydentate-I and -II, on all sodium promoted samples, respectively (see Supporting Information, Figure S4).[43,44] The interaction of gaseous CO_2 with the sorbents was monitored with in situ IR spectroscopy, and the IR spectra in Figure 2 indicate that three new surface carbonates are formed during CO_2 adsorption at 200 °C. Bicarbonate species (HCO_3–Al) are present on samples below sodium monolayer coverage (bare Al_2O_3 and 1–3% Na_2O/Al_2O_3) with bands at 1650 (ν_{3as}), 1436 (ν_{3s}), and 1225 cm^{-1} (δ_{OH}).[20,43,45–52] In addition, on all sodium containing samples two different bidentate carbonate (OCO_2-μ_1-Al) groups, labeled bidentate-I and -II, are observed with bands at 1677 (ν_{3as}) + 1376 cm^{-1} (ν_{3s}) and 1625 (ν_{3as}) + 1311 cm^{-1} (ν_{3s}), respectively. It is not immediately obvious that two surface bidentate species exist, however, operando TP-IR data easily resolves the two surface bicarbonates because of their different desorption kinetics, as shown below.

It is well known that CO_2 (a weak acid/electrophile) adsorbs as a surface bicarbonate species via nucleophilic attack between an alumina hydroxyl and CO_2, which has recently been supported by quantum chemical calculations.[53] Despite the presence of five easily observable surface hydroxyl types (Table S1), only a single surface bicarbonate species is observed on bare γ-alumina (at 200 °C) and this oxide's CO_2 working capacity can increase by nearly six times with the addition of sodium. These experimental observations indicate that not all γ-alumina hydroxyls possess a strong enough basic character at 200 °C to form surface carbonate species with CO_2. Carbon dioxide adsorption at room temperature on γ-alumina, however, has shown the presence of more than just surface bicarbonate species.[20,54–57]

The operando TP-IR spectroscopy results, presented in Figure 3, provide direct monitoring of the different surface carbonate species on the sorbent during CO_2-temperature-programmed desorption (TPD). In Figure 3B, bands corresponding to a surface bicarbonate species (HCO_3–Al, blue labels) decrease dramatically between 100–200 °C, correlating very well with the observed 124 °C CO_2 desorption peak in the mass spectrum, 1% Na_2O/Al_2O_3 in Figure 3A. Sorbents at monolayer coverage or above, ~5–9% Na_2O/Al_2O_3, possess a second CO_2 desorption peak at 255 °C as well as a low temperature peak at 150 °C. The 255 °C CO_2 desorption peak correlates quite well with IR bands for the surface bidentate-II species (OCO_2-μ_1-Al, red II-labels), Figure 3D–F, that begin to decrease in intensity around 200 °C and never completely disappear. Since surface bicarbonates are no longer observed at these high Na_2O loadings, the low temperature CO_2 desorption peak at 150 °C is attributed to a surface bidentate-I species (OCO_2-μ_1-Al, red I-labels) whose bands decrease rapidly between 100–200 °C,

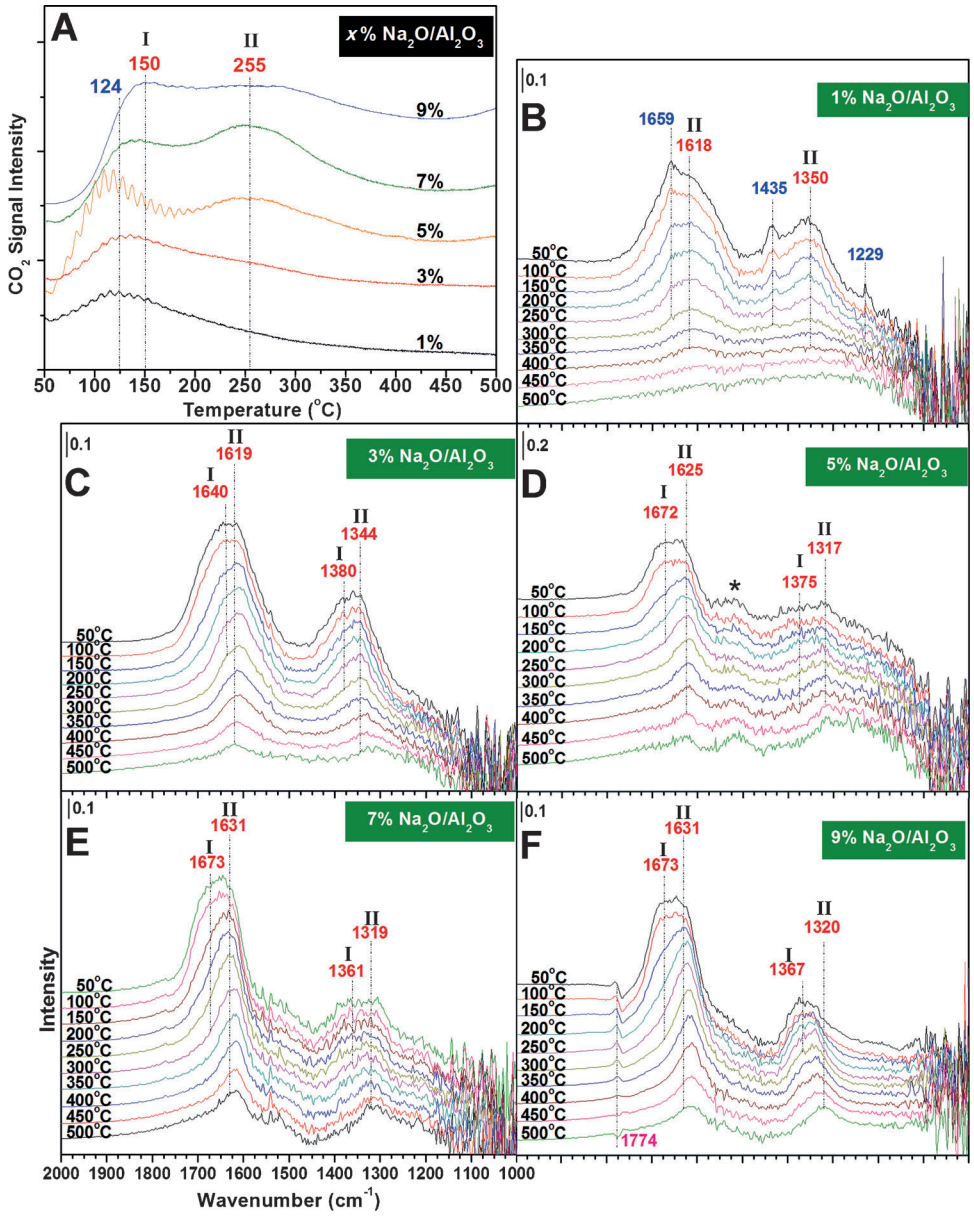

Figure 3. Operando TP-IR spectroscopy of CO_2 adsorption on x% Na_2O/Al_2O_3. A) Mass spectroscopy CO_2-TPD curves from sorbents ($m/e = 44$), B) DRIFTS spectra of 1% Na_2O/Al_2O_3, C) 3% Na_2O/Al_2O_3, D) 5% Na_2O/Al_2O_3, E) 7% Na_2O/Al_2O_3, and F) 9% Na_2O/Al_2O_3. (B)–(F) have the same x-axis as (E). The dehydrated spectrum of each sample before CO_2 adsorption was subtracted from all spectra during CO_2 TPD. Bands labeled with a "*" are artifacts resulting from spectral subtraction.

As previously discussed, the formation of surface Al–O^- ionic sites in place of surface hydroxyls, via sodium doping, imparts a greater nucleophilic/basic character to the oxygen atoms of alumina. Furthermore, we experimentally observe that sodium doping titrates all five observable alumina surface hydroxyls and causes the formation of additional carbonates species with surface bidentate (OCO_2-μ_1-Al) and surface polydentate (CO_3-μ_3-Al) coordinations. This is clear evidence that the addition of sodium converts otherwise inactive surface hydroxyls (weak nucleophiles/bases) into active surface Al–O^-, ions (strong nucleophiles/bases) that can complex with CO_2, Scheme 1. The different Al–OH/Al–O^- coordination on γ-alumina give rise to surface carbonates that also vary in their coordination. In situ and operando spectroscopy data also reveal that some surface hydroxyls convert into Al–O^- groups that are too strongly nucleophilic/basic in character, forming extremely stable surface carbonate groups that do not desorb at temperatures as high as 500 °C (surface polydentates).

A summary of all experimentally observed surface carbonates on γ-alumina and Na_2O/alumina is given in Table 2. It is difficult to experimentally distinguish which surface carbonate species bond to a specific hydroxyl/ionic sites since several different surface hydroxyls are most easily observed in Figure 3D and 3F. A negative IR band is also present at 1774 cm^{-1} in Figure 3F, previously assigned to Na_2CO_3 NPs, indicating irreversible decomposition of Na_2CO_3 NPs that can release CO_2. On several sorbents it appears that surface bidentate-II carbonates do not fully desorb from the surface, which suggests there may be more than just the two observed surface bidentate carbonates, with subtle differences between them. consumed simultaneously upon the addition of a small amount of sodium. It is also extremely likely that there are

Table 2. Summary of surface carbonates detected on the Na_2O/Al_2O_3 sorbents.

Sorbent	Species	Desorption temperature [°C]	ν_{3as} (O–C–O) [cm^{-1}]	ν_{3s} (O–C–O) [cm^{-1}]	δ_{OH} [cm^{-1}]	$\Delta\nu_3$ [cm^{-1}]
Al_2O_3	bicarbonate	124	1650	1436	1225	214
Na_2O/Al_2O_3	polydentate-I	> 500	1571	1353	–	218
	polydentate-II	> 500	–	1450	–	–
	bidentate-I	150	1672–1677	1361–1376	–	301–311
	bidentate-II	255	1618–1631	1311–1320	–	307–312

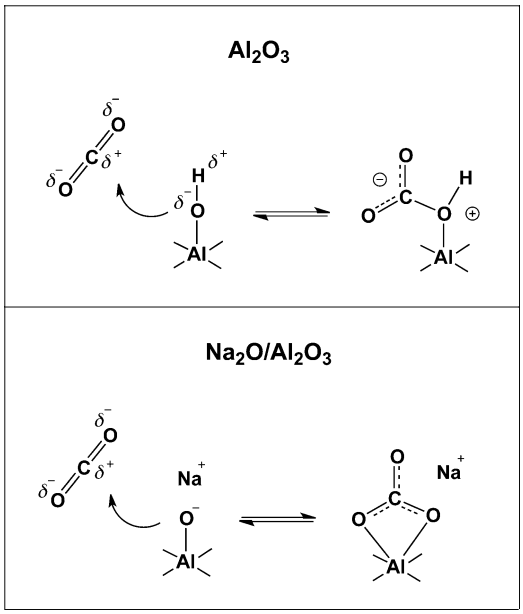

Scheme 1. Top: Diagram illustrating nucleophilic attack between an alumina hydroxyl and CO_2 to form a bicarbonate species. Bottom: Diagram illustrating nucleophilic attack between an Al–O^- group and CO_2 to form a bidentate carbonate species.

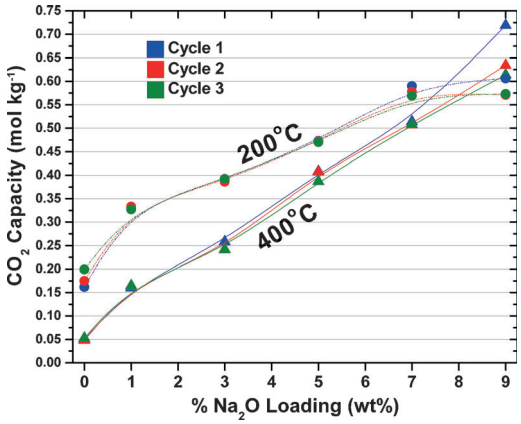

Figure 4. CO_2 capacity of x% Na_2O/Al_2O_3 sorbents calculated based on TGA weight analysis at two different adsorption/desorption temperatures. Each sorbent completed three adsorption/desorption cycles for reproducibility.

more surface hydroxyl types present on γ-Al_2O_3, in addition to the five surface hydroxyls detected in the IR spectra, especially given that Digne et al. has computed over 10 unique, stable surface hydroxyls on γ-Al_2O_3.[39,40]

It is hypothesized that the formation of extremely basic (nucleophilic) surface Al–O^- ionic sites is a general phenomenon of alkali metal chemistry and metal-oxide surfaces. Early studies examining Li-, Na-, and K-promoted alumina found that basicity positively correlates with the alkali metal ionic radius, that is, Li-alumina < Na-alumina < K-alumina.[35,36] This hypothesis is supported by CO_2 heats of adsorption of many alkali and alkaline earth metals on γ-alumina, as measured by Horiuchi et al.[55] They found that all tested alkali metals (Na, K, Rb, Cs) gave the highest heats of adsorption (≈160–170 kJ mol^{-1}) compared to alkaline earth metals (Mg, Ca, Sr, Ba; ≈140–170 kJ mol^{-1}) and rare earth metals (La, Ce, Pr, Nd; ~110–140 kJ mol^{-1}) of similar loading on γ-alumina (bare γ-alumina ~80 kJ mol^{-1}). These data would be much more potent if the measured surface densities of each dopant were used to normalize the heats of adsorption, (instead of assuming all loadings were similar), but it makes the point that alkali metal dopants create surface sites with greater basicity on γ-alumina.

The CO_2 adsorption working capacity of the synthesized sorbents, calculated from TGA weight analysis, is presented in Figure 4 and the maximum rate of adsorption is presented in Figure S5. The sorbents underwent three cycles of CO_2 adsorption/desorption at both 200 and 400 °C, to ensure accuracy of the measured CO_2 adsorption capacities.

For an adsorption temperature of 200 °C, the CO_2 adsorption capacity increases with Na loading and plateaus at 7% Na_2O/Al_2O_3 (monolayer coverage). The maximum rate of adsorption at 200 °C parallels this trend. For adsorption at 400 °C, the CO_2 adsorption capacity increases with Na loading and does not plateau. The maximum rate of adsorption at 400 °C parallels this trend as well. Although 200 °C is a better temperature for maximizing the overall CO_2 working capacity of the sorbents, the gap between the capacity at 200 °C and 400 °C narrows significantly until 7% Na_2O/Al_2O_3, at which point a crossover happens. The CO_2 adsorption capacity of the 9% Na_2O/Al_2O_3 sorbent shows significant variability at 400 °C, with a large decrease from 0.72–0.60 mol kg^{-1} during the three cycles of adsorption/desorption.

The new molecular level insights gained from in situ and operando spectroscopy allows us to understand the CO_2 working capacity trends of the Na_2O/Al_2O_3 sorbents presented in Figure 4. Through operando TP-IR spectroscopy, it was demonstrated that the surface bicarbonate and surface bidentate-I carbonate species are responsible for the majority of the CO_2 capacity at 200 °C since bidentate-II species desorb around 255 °C. An adsorption temperature of 400 °C is too high to utilize the surface bicarbonates and surface bidentate-I species, which would instantly desorb upon formation. Consequently, the CO_2 capacity at 400 °C is generally lower. For 7% Na_2O/Al_2O_3, the CO_2 capacities are nearly equal due to a nearly equal amount of surface bidentate-I and surface bidentate-II species, based on the desorption curve intensity of Figure 3 A. The surface bidentate-II species, however, desorb around 255 °C, which is much lower than the 400 °C adsorption temperature, suggesting that there are more than just these two observable, reversible surface bidentate carbonates contributing to the CO_2 capacity.

At high loadings of 7 and 9% Na_2O/Al_2O_3, both the CO_2 working capacity and maximum adsorption rate trends plateau with a 200 °C adsorption temperature, but increase linearly with a 400 °C temperature. The trend with a 400 °C adsorption temperature indicates that new, high-temperature reversible sites are being formed on the sorbents, despite no spectral evidence of new surface carbonate species, only Na_2CO_3 3D NPs. Thus, it appears that Na_2CO_3 NPs provide additional, high-temperature reversible adsorption sites, presumably via the negatively charged carbonate ion (CO_3^{2-}), however, in situ IR spec-

tra of CO_2 adsorption on bulk Na_2CO_3 revealed no carbonate bands due to the bulk compounds low surface area.

Carbon dioxide adsorption on an ionic carbonate crystal should tend to have no single adsorption site due to the equal charge distribution around the carbon atom and the heterogeneous nature of the surfaces of NPs, and, thus, should possess multiple sites with different binding energies, depending on the local environment around a negative oxygen atom. Our CO_2 working capacity data support this hypothesis, which is most evident through analysis of the shape of the CO_2 TPD curve for 9% Na_2O/Al_2O_3 (Figure 3 A), which is flat and no longer has easily distinguishable desorption peaks at 155 and 255 °C. Furthermore, the observed decomposition of the Na_2CO_3 NPs (Figure 3 F) between each adsorption–desorption cycle (there is a 550 °C calcination step between each total cycle) explains the decrease in capacity for 9% Na_2O/Al_2O_3 after three cycles. Note that the CO_2 capacity at 200 °C for 7 and 9% Na_2O/Al_2O_3 is the same because monolayer coverage has been achieved (no new adsorption sites) and the Na_2CO_3 NPs possess mostly high-temperature adsorption sites. This is the first study to monitor the dynamics of CO_2 capture at high temperatures on metal-oxide sorbents. The detailed mechanistic insight gained from the operando spectroscopy approach indicates that the rational synthesis of advanced metal-oxide sorbents should focus on maximizing the utilization of surface hydroxyl groups for low temperature applications and carbonate nanoparticles for high temperature applications.

Conclusions

Na_2O/Al_2O_3 sorbents were synthesized via the incipient wetness impregnation method and were studied by means of operando TP-IR spectroscopy, in situ Raman spectroscopy, and TGA analysis. Addition of the sodium promoter consumed five observable γ-Al_2O_3 surface hydroxyls and experimental evidence suggests the formation of (more basic) surface Al–O^- ionic sites in place of the surface hydroxyls. Sodium monolayer coverage was determined to be 6–7 wt% Na_2O, with the formation of ionic Na_2CO_3 crystalline NPs seen at 7% Na_2O and above. The in situ adsorption of CO_2 revealed that bare γ-alumina forms only reversible bicarbonate species at 200 °C because most surface hydroxyls are too weakly basic to form stable carbonates. The addition of sodium and formation of Al–O^- ionic sites allowed many more hydroxyl sites to be accessed for CO_2 capture, with Na_2O/Al_2O_3 sorbents forming bidentate and polydentate carbonates. It is hypothesized that hydroxyl conversion into basic surface M-O^- ionic sites is a general phenomenon arising from the ionic nature of alkali metal chemistry.

Operando TP-IR spectroscopy revealed that bicarbonates, bidentate-I, and bidentate-II carbonate species are responsible for CO_2 desorption peaks at 124, 150, and 255 °C respectively, and the majority of the CO_2 working capacity of the sorbents when utilized at 200 °C. Experimental data suggests, however, that there could be more than just the three major reversible carbonates that were observed. Additionally, it was observed that surface ionic Na_2CO_3 NPs possess multiple adsorption sites with different binding energies, due to their heterogeneous nature, which can reversibly adsorb CO_2 at higher temperatures than Al–O^- sites. These NPs can also thermally decompose at high temperatures, irreversibly releasing CO_2. These new insights into the CO_2 capture mechanism indicate that the rational synthesis of advanced metal-oxide sorbents should focus on maximizing the utilization of surface hydroxyl groups for low-temperature applications and carbonate nanoparticles for high-temperature applications.

Experimental Section

Sorbent synthesis and preparation: The supported Na_2O alumina sorbents were prepared by incipient wetness impregnation of aqueous solutions of sodium hydroxide (NaOH, Fisher Scientific, 97.8%) and deionized water on an alumina support (γ-Al_2O_3, 200 $m^2 g^{-1}$, Engelhard). The alumina support underwent calcination at 500 °C for 4 h in air (Airgas, Zero grade) prior to impregnation. Samples were impregnated with sodium loadings of 1, 2, 3, 5, 7, and 9 wt% Na_2O. The samples were allowed to dry overnight under ambient conditions, followed by a second drying step in flowing air (100 mL min^{-1}) at 100 °C for 4 h in a programmable furnace (Thermolyne, Model 48000). Finally, the samples were subjected to calcination by ramping the temperature at 5 °C min^{-1} under flowing air (Airgas, Zero grade) to 400 °C for 2 h. The final synthesized sorbents are denoted as x% Na_2O/Al_2O_3, where x = weight% of sodium oxide.

Surface area analysis: The quantity of sample used for the adsorption experiments was chosen to match an approximate sample size of 1000 $m^2 g^{-1}$. Measurements were performed using the Micromeritics ASAP 2020 Surface Area and Porosity Analyzer. The catalysts were initially degassed for 12 h at 350 °C before adsorption measurements. For surface area analysis, a N_2-adsorption study was performed. An adsorption isotherm was obtained at different relative pressures (P_0/P from 0.01 to 1.0) with the sample submerged in liquid N_2. The BET method was used to obtain the specific surface area for the samples and was conducted using the software provided by Micromeritics.

CO_2 sorption working capacity and maximum adsorption rate: A TA instruments SDT Q600 was used for the TGA analysis. Nitrogen (Praxair, > 99.998%) was used as the purge gas and CO_2 (Praxair, > 99.998%) for adsorption steps. A typical TGA run was carried out with around 30 mg powder using platinum pans at 1 atm. In a typical cycle, the sample was first heated at 5 °C min^{-1} to 550 °C and kept at that temperature for 4 h in 100 mL min^{-1} flowing N_2 in order to dehydrate the sample and desorb residual CO_2. During the adsorption step the temperature was equilibrated to 400 °C and the gas was switched to 60 mL min^{-1} flowing CO_2 for 4 h. The influence of flow rate change is negligible and was confirmed by checking the weight signal change using empty platinum pans. During the desorption step the gas was switched to 100 mL min^{-1} flowing N_2 at the same temperature for 5 h. With a N_2 purge, the temperature was equilibrated at 200 °C and the gas was switched to 60 mL min^{-1} flowing CO_2 for 4 h, followed by desorption under N_2 for 5 h. These steps outline one adsorption/desorption cycle. Each of the samples was tested for the three complete cycles.

The maximum adsorption rate of CO_2 was determined from the derivative of the TGA weight versus time curve for only the first cycle. The derivative was calculated using a seven point Savitsky–Golay method implemented in Microsoft Excel. The maximum derivative value was taken as the maximum adsorption rate.

In situ diffuse reflectance infrared Fourier transform spectroscopy (DRIFTS) of dehydrated sorbents: The in situ IR spectra of the sorbents were obtained with a Thermo Nicolet 8700 FT-IR spectrometer equipped with a Harrick Praying Mantis attachment (model DRA-2) for diffuse reflectance spectroscopy. Approximately 30 mg of each sample (powder) was loaded into the cup of the high temperature Harrick cell (model HVC-DR2 with a ZnSe window). The sample was initially heated at a rate of 10 °C min^{-1} (Harrick ATC/low voltage temperature control unit) in the Harrick cell to 400 °C and held for 45–60 min under 30 mL min^{-1} flowing 10% O_2/Ar (Airgas, certified, 10.00% O_2/Ar balance) before cooling to 200 °C. The in situ IR spectra were collected at 200 °C using an MCT detector (cooled with liquid N_2) with a resolution of 4 cm^{-1} and an accumulation of 72 scans (≈90 s per scan).

The collection of the initial IR gas phase background was performed by placing a reflective mirror in the laser path, while using the Harrick Praying Mantis attachment, at approximately the same height as a full sample cup of the Harrick Cell. A new background was taken for each sample.

In situ DRIFTS of CO_2 adsorption: The adsorption of CO_2 was performed after collecting a DRIFTS spectrum of each dehydrated sample at 200 °C. This adsorption temperature was chosen based on sorbent operating temperatures in SER technology.[1] After the in situ DRIFTS spectrum was collected at 200 °C, the gas was switched to 5 mL min^{-1} of flowing CO_2 (Airgas, bone dry grade). The sample was held in this environment for one hour. A macro was made using the program OMNIC Macros/Basic to continuously collect spectra for the full hour. With a resolution of 4 cm^{-1} and 72 scans, each spectrum took approximately one minute and thirty seconds to collect, giving roughly 40 spectra for the full hour. The DRIFTS spectrum of each dehydrated sample was subtracted from all 40 spectra (performed in OMNIC, subtraction factor = 1) so that only the vibrations of the adsorbed CO_x species are observed.

Operando temperature programmed-IR spectroscopy: A mass spectrometer (Pfeiffer Quadrupole Mass Spectrometer, Model QME200) was attached to the outlet stream of the Harrick cell in order to monitor the exiting gas phase while simultaneously obtaining in situ DRIFTS spectra of the sample. The mass spec vacuum was maintained around 5.1×10^{-9} atm. The activation and CO_2 adsorption procedure used were identical to that previously reported above. After a full hour of CO_2 adsorption at 200 °C, the sample was allowed to cool to 50 °C under the flowing CO_2 atmosphere. Once at 50 °C, the gas was switched to argon (Airgas, UHP) at a flow of 30 mL min^{-1}. The sample was maintained at 50 °C under the argon flow for ~30 min to help eliminate any physisorbed species and allow the mass spec to reach a baseline value for each mass monitored. Afterwards, the sample temperature was ramped from 50 °C to 500 °C at 10 °C min^{-1}. The mass spec was set to continuously analyze the exiting CO_2 gas and the IR system was set to record a spectrum every ~90 s. The corresponding in situ DRIFTS spectra of the dehydrated sorbents were subtracted from all spectra taken during CO_2-TPD (performed in OMNIC, subtraction factor = 1). This allows for spectral examination of the desorption behavior of only the adsorbed species.

Acknowledgements

We would like to thank Professor Mark A. Snyder of Lehigh University for use of TGA equipment and Air Products Inc. for the donated industrial sorbents for comparison. Funding was provided by the Department of Energy (DOE), grant DE-PS26-O4NT-42454, the Pennsylvania Infrastructure Technology Alliance (PITA), grants PITA-442-04 & PITA-542-5, and NSF-REU grant #0609018.

Keywords: carbon dioxide capture · IR spectroscopy · operando spectroscopy · sorbent · surface chemistry

[1] K. Lee, M. Beaver, H. Caram, S. Sircar, *Ind. Eng. Chem. Res.* **2008**, *47*, 8048.
[2] S. Choi, J. H. Drese, C. W. Jones, *ChemSusChem* **2009**, *2*, 796–854.
[3] B. T. Carvill, J. R. Hufton, M. Anand, S. Sircar, *AIChE J.* **1996**, *42*, 2765.
[4] K. B. Lee, M. G. Beaver, H. S. Caram, S. Sircar, *AIChE J.* **2007**, *53*, 2824–2831.
[5] K. Lee, M. Beaver, H. Caram, S. Sircar, *Adsorption* **2007**, *13*, 385.
[6] K. B. Lee, M. G. Beaver, H. S. Caram, S. Sircar, *J. Power Sources* **2008**, *176*, 312–319.
[7] M. G. Beaver, H. S. Caram, S. Sircar, *J. Power Sources* **2010**, *195*, 1998–2002.
[8] T. R. Gaffney, T. C. Golden, S. G. Mayorga, J. R. Brzozowski, F. W. Taylor, **1999**.
[9] J. R. Hufton, S. G. Mayorga, S. Sircar, *AIChE J.* **1999**, *45*, 248–256.
[10] S. Sircar, C. Golden, **2001**.
[11] W. E. Waldron, J. R. Hufton, S. Sircar, *AIChE J.* **2001**, *47*, 1477.
[12] S. K. Bhatia, D. D. Perlmutter, *AIChE J.* **1983**, *29*, 79–86.
[13] B. Balasubramanian, A. L. Ortiz, S. Kaytakoglu, D. P. Harrison, *Chem. Eng. Sci.* **1999**, *54*, 3543–3552.
[14] A. A. G. Belova, T. M. Yegulalp, C. T. Yee, *Energy Procedia* **2009**, *1*, 749–755.
[15] P. Gruene, A. G. Belova, T. M. Yegulalp, R. J. Farrauto, M. J. Castaldi, *Ind. Eng. Chem. Res.* **2011**, *50*, 4042–4049.
[16] Z. Zhou, Y. Qi, M. Xie, Z. Cheng, W. Yuan, *Chem. Eng. Sci.* **2012**, *74*, 172–180.
[17] N. Amos, M. Widyawati, S. Kureti, D. Trimis, A. I. Minett, A. T. Harris, T. L. Church, *J. Mater. Chem. A* **2014**, *2*, 4332–4339.
[18] M. S. Duyar, R. J. Farrauto, M. J. Castaldi, T. M. Yegulalp, *Ind. Eng. Chem. Res.* **2014**, *53*, 1064–1072.
[19] M. A. Vuurman, I. E. Wachs, *J. Phys. Chem.* **1992**, *96*, 5008.
[20] A. M. Turek, I. E. Wachs, E. Decanio, *J. Phys. Chem.* **1992**, *96*, 5000.
[21] I. E. Wachs, *Colloids Surf. A* **1995**, *105*, 143.
[22] I. E. Wachs, *Catal. Today* **1996**, *27*, 437–455.
[23] X. Liu, R. Truitt, *J. Am. Chem. Soc.* **1997**, *119*, 9856.
[24] I. E. Wachs, Y. Chen, J.-M. Jehng, L. E. Briand, T. Tanaka, *Catal. Today* **2003**, *78*, 13–24.
[25] I. E. Wachs, *Catal. Today* **2005**, *100*, 79–94.
[26] G. Crépeau, V. Montouillout, A. Vimon, L. Mariey, T. Cseri, F. Mauge, *J. Phys. Chem. B* **2006**, *110*, 15172.
[27] I. E. Wachs, C. J. Keturakis in *Monolayer Systems, Vol. 7* (Ed.: R. Schlögl), Elsevier, **2013**.
[28] A. R. Saini, B. G. Johnson, F. E. Massoth, *Appl. Catal.* **1988**, *40*, 157–172.
[29] V. Bolis, G. Magnacca, C. Morterra, *Res. Chem. Intermed.* **1999**, *25*, 25–56.
[30] H. Dathe, A. Jentys, P. Haider, E. Schreier, R. Fricke, J. A. Lercher, *Phys. Chem. Chem. Phys.* **2006**, *8*, 1601–1613.
[31] X. Wang, I. E. Wachs, *Catal. Today* **2004**, *96*, 211–222.
[32] F. Prinetto, M. Manzoli, S. Morandi, F. Frola, G. Ghiotti, L. Castoldi, L. Lietti, P. Forzatti, *J. Phys. Chem. C* **2010**, *114*, 1127–1138.
[33] D. H. Kim, K. Mudiyanselage, J. Szanyi, J. C. Hanson, C. H. F. Peden, *J. Phys. Chem. C* **2014**, *118*, 4189–4197.
[34] M. E. Gálvez, S. Ascaso, P. Stelmachowski, P. Legutko, A. Kotarba, R. Moliner, M. J. Lazaro, *Appl. Catal. B* **2014**, *152–153*, 88–98.
[35] R. Fiedorow, I. G. Dalla Lana, *J. Phys. Chem.* **1980**, *84*, 2779–2782.
[36] P. O. Scokart, A. Amin, C. Defosse, P. G. Rouxhet, *J. Phys. Chem.* **1981**, *85*, 1406–1412.
[37] V. B. Kazansky, A. V. Zaitsev, V. Y. Borovkov, A. L. Lapidus, *Appl. Catal.* **1988**, *40*, 17–25.
[38] V. A. Ivanov, A. Pieplu, J. C. Lavalley, P. Nortier, *Appl. Catal. A* **1995**, *131*, 323–334.
[39] M. Digne, P. Sautet, P. Raybaud, P. Euzen, H. Toulhoat, *J. Catal.* **2002**, *211*, 1–5.

[40] M. Digne, P. Sautet, P. Raybaud, P. Euzen, H. Toulhoat, *J. Catal.* **2004**, *226*, 54 – 68.
[41] H. R. Watling, P. M. Sipos, L. Byrne, G. T. Hefter, P. M. May, *Appl. Spectrosc.* **1999**, *53*, 415 – 422.
[42] D. McKeown, *Am. Mineral.* **2005**, *90*, 1506 – 1517.
[43] G. Busca, V. Lorenzelli, *Mater. Chem.* **1982**, *7*, 89.
[44] P. Nortier, P. Fourre, A. B. M. Saad, O. Saur, J. C. Lavalley, *Appl. Catal.* **1990**, *61*, 141 – 160.
[45] J. B. Peri, *J. Phys. Chem.* **1966**, *70*, 3168 – 3179.
[46] N. D. Parkyns, *J. Chem. Soc. A* **1969**, 410 – 417.
[47] E. Baumgarten, A. Zachos, *Spectrochim. Acta* **1981**, *37A*, 93 – 98.
[48] D. G. Rethwisch, J. A. Dumesic, *Langmuir* **1986**, *2*, 73 – 79.
[49] D. G. Rethwisch, J. A. Dumesic in *Adsorptive and Catalytic Properties of Carbon Monoxide and Carbon Dioxide Over Supported Metal Oxides, Vol. 363* (Ed.: W. M. Ayers), American Chemical Society, **1988**, pp. 102 – 122.
[50] M. Cabrejas Manchado, J. M. Guil, A. P. Masia, A. R. Paniego, J. M. T. Menayo, *Langmuir* **1994**, *10*, 685 – 691.
[51] H. Zou, X. Ge, J. Shen, *Thermochim. Acta* **2003**, *397*, 81 – 86.
[52] A. Vimont, J. C. Lavalley, A. Sahibed-Dine, C. O. Arean, M. R. Delgado, M. Daturi, *J. Phys. Chem. B* **2005**, *109*, 9656 – 9664.
[53] J. Baltrusaitis, J. H. Jensen, V. H. Grassian, *J. Phys. Chem. B* **2006**, *110*, 12005 – 12016.
[54] P. Galhotra, **2010**.
[55] T. Horiuchi, H. Hidaka, T. Fukui, Y. Kubo, M. Horio, K. Suzuki, T. Mori, *Appl. Catal. A* **1998**, *167*, 195 – 202.
[56] J. I. Di Cosimo, V. K. Diez, M. Xu, E. Iglesia, C. R. Apesteguia, *J. Catal.* **1998**, *178*, 499 – 510.
[57] S. Walspurger, L. Boels, P. Cobden, G. Elzinga, W. Haije, R. van den Brink, *ChemSusChem* **2008**, *1*, 643.

Received: May 31, 2014
Revised: August 22, 2014
Published online on October 21, 2014